Dephasing in single-electron generation due to environmental noise probed by Hong Ou Mandel interferometry

Eiki Iyoda,[1,*] Takeo Kato,[2] Kazuki Koshino,[3] and Thierry Martin[4]

[1]*Department of Basic Science, University of Tokyo, 3-8-1 Komaba, Meguro, Tokyo 153-8902, Japan*
[2]*Institute for Solid State Physics, University of Tokyo, Kashiwa, Chiba 277-8581, Japan*
[3]*College of Liberal Arts and Sciences, Tokyo Medical and Dental University, Ichikawa, Chiba 272-0827, Japan*
[4]*Aix Marseille Université, Université de Toulon, CNRS, CPT, UMR 7332, 13288 Marseille, France*

(Dated: May 9, 2014)

We consider the effect of dephasing on a quantum dot which injects single electrons on a chiral edge channel of the quantum Hall effect. Dephasing is described by the coupling of the dot to a bosonic bath which represents the electromagnetic environment. Using the input-output formalism of quantum optics, we derive the density matrix of the edge degrees of freedom. Results are illustrated by computing the zero frequency current-current correlations when two such single electron emitters achieve a collision at the location of a quantum point contact, in the same spirit as the Hong Ou Mandel experiment of quantum optics. Such correlations are directly linked to the quantum mechanical purity. We show that as observed in a recent experiment, the effect of dephasing leads to a lifting of the Hong Ou Mandel dip when the time delay between the two electron wave packets is zero. Generalizations to time filtered wave packets as well as to asymmetric, detuned injection between opposite edges are obtained.

PACS numbers:

I. INTRODUCTION

Quantum mesoscopic physics, or nanophysics, aims at studying the manifestations of quantum mechanics, such as interference effects and coherence, with electron transport in condensed matter materials. Such manifestations have been studied in the context of quantum optics since the middle of the last century, where fundamental tests of quantum mechanics were explored, for instance in Hanbury Brown and Twiss[1] (HBT) and Hong Ou Mandel[2] (HOM) experiments, more recently with single photon sources.[3] In nanophysics, there is a growing interest to translate these concepts of quantum optics to electrons propagating in nanostructures. To a large extent, this is due to the recent availability of on-demand single electron sources,[4–9] and of material which acts as wave guides for the electrons, such as edge states in the quantum Hall effect. Electrons differ from photons because of their fermionic statistics, in condensed matter settings they are always accompanied by a Fermi sea, and as charged particles they interact strongly between themselves and with their environment.

In electronic quantum optics, the fermionic counterpart of the Hong-Ou-Mandel(HOM) experiment[2] has been considered theoretically in a setup of a two-electron collider,[10,11] and has been realized quite recently in the integer quantum Hall effect regime[12] and in a point contact system using levitons.[13] Nonlocal quantum correlation between propagating electrons in conduction channels and related nonlocal transport have also been studied theoretically towards applications to quantum information processing.[14,15]

The experiments of on-demand electron generation in electronic transmission channels have stimulated the theoretical study on the quantum-mechanical nature of the single electrons which are generated in the one-dimensional channel.[16–29] The excess current noise at the output of a quantum point contact (QPC), which includes the information about the coherence of generated electrons, has been studied both theoretically and experimentally.[30–33] This coherence is directly measured by the degree of antibunching in the fermonic HOM experiment, which reflects the indistinguishability of electrons. The imperfect antibunching reported in Ref. 12 (the fact that the HOM dip is lifted for zero time delay between electron wave packets) includes information about the distinguishability of propagating electrons in the chiral edge channels before arriving at the collision point (the QPC) as well as asymmetry of the wave packet due to difference in parameters of two single-electron generator.

At the present, the dephasing of propagating electrons within propagating channels has been considered mostly by phenomenological approaches,[34] by ad-hoc fitting of the experimental curves,[12] or alternatively using the bosonization approach.[35,36] In these works, the relaxation due to Coulomb interaction between an edge state at its electromagnetic environment or between propagating edge channels[37–41] is assumed to be the main source of decoherence.

Yet, there are many other possibilities for other sources of decoherence, among them the simple fact that the metallic gates surrounding the dot represent a fluctuating electromagnetic environment. In this paper, we examine the effect of electron decoherence by focusing on the role of the energy-level fluctuations of the quantum dot due to this environment. We present a simple framework for evaluating the quality of the generated

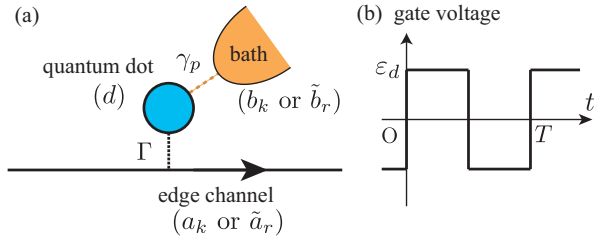

FIG. 1: (a) Schematic picture of the model considered in this paper: a quantum dot (blue) which is coupled to an electromagnetic environement (orange) is subject to a periodic drive in order to transfer electrons on the neighboring chiral edge state. (b) The square periodic voltage pulse which is applied to the quantum dot.

electrons reflecting indistinguishability of electrons based on the so-called input-output relation, which is a standard tool in quantum optics.[42–47] To our knowledge, the input-output relations have so far not been applied to a fermonic quantum optics setup. Our calculation provides a useful and comprehensive picture of dephasing effects on the quality of generated single electrons as well as simple formulae for the degree of antibunching in the HOM experiment. Finally, we also show that the decoherence due to the energy-level fluctuation at the quantum dot can be reduced by a filtering technique.

II. MODEL

In actual experiments, the single electron source consists of a mesoscopic capacitor[48] which is a rather "large"[49] quantum dot, connected to a quantum Hall edge channel propagating in one direction. The dot is controlled by an electrostatic gate, and its energy levels are understood to be dominated by confinement rather than Coulomb charging energy. For our purposes, we thus choose to describe it as a single level dot coupled to both a chiral edge channel of the integer quantum Hall states, and a bosonic bath representing the electromagnetic environment, as illustrated in Fig. 1. The Hamiltonian is thus given by:

$$H = \varepsilon_d n_d + \int dk\, k a_k^\dagger a_k + \sqrt{\Gamma}(d^\dagger \tilde{a}_0 + \tilde{a}_0^\dagger d) + \int dk\, k b_k^\dagger b_k + \sqrt{2\gamma_p}(n_d \tilde{b}_0 + \tilde{b}_0^\dagger n_d)\ , \tag{1}$$

where d, a_k and b_k are annihilation operators of the dot electron, the edge-state electrons, and the bosonic degrees of freedom, respectively, the dot occupation is $n_d = d^\dagger d$, and spin degrees of freedom have been neglected assuming that electrons are fully polarized. Here, ε_d, Γ and γ_p are the energy level of the quantum dot, the decay rate of the dot electron, and the pure dephasing rate, respectively. The velocity of the edge-channel electrons and the environment bosons has been set to be unity. We have introduced the real-space representations:

$$\tilde{a}_r = \frac{1}{\sqrt{2\pi}} \int dk\, a_k e^{ikr}\ , \tag{2}$$

$$\tilde{b}_r = \frac{1}{\sqrt{2\pi}} \int dk\, b_k e^{ikr}\ . \tag{3}$$

The integral over the bosonic bath is assumed to be taken in the range $-\infty < k < \infty$. This assumption leads to simple Markov dynamics for the electron dynamics in the quantum dot:[47] the fluctuating potential energy acting on the dot is then characterized by a white noise spectrum. Throughout this paper, we set $\hbar$ to unity.

III. INPUT-OUTPUT RELATIONS

In this paper, we calculate the density matrix of single electrons (holes) injected from a quantum dot subjected to an alternating gate voltage [shown in Fig. 1 (b)], at zero temperature.[50] We assume that the period T of the alternating field is much larger than the decay time Γ^{-1} of the electrons escaping the dot, and simultaneously that the change of the field is sufficiently fast compared with Γ^{-1}. Then, the initial state at $t = 0$ in Fig. 1 (b) is given by $|\psi(0)\rangle = |n_d = 1\rangle \otimes |\mathrm{FS}\rangle \otimes |\mathrm{vac}\rangle$, where $|\mathrm{FS}\rangle$ denotes the ground state of the chiral edge channel (the Fermi sea), and $|\mathrm{vac}\rangle$ denotes the vacuum state of the environment Hamiltonian at $t < 0$, for which the occupation and electron hopping are fixed as $n_d = 1$ and $\Gamma = 0$, respectively (for details, see Appendix A). In the following, we consider electron injection occurring in the interval $0 < t < T/2$, as the hole injection occurring in $T/2 < t < T$ can be regarded as an independent dynamics that gives the same contribution to the excess noise. We first derive the input-output relations, and then utilize them to calculate the various quantities which characterize the injected electrons.

For the derivation of the input-output relations, we use the equations of motion in the Heisenberg picture:

$$i\dot{a}_k(t) = [a_k, H] = k a_k + \sqrt{\Gamma/2\pi} d\ , \tag{4}$$

$$i\dot{b}_k(t) = [b_k, H] = k b_k + \sqrt{\gamma_p/\pi} n_d\ . \tag{5}$$

They are formally solved as:

$$a_k(t) = a_k(0) e^{-ikt} - i\sqrt{\frac{\Gamma}{2\pi}} \int_0^t dt' d(t') e^{ik(t'-t)}\ , \tag{6}$$

$$b_k(t) = b_k(0) e^{-ikt} - i\sqrt{\frac{\gamma_p}{\pi}} \int_0^t dt' n_d(t') e^{ik(t'-t)}\ , \tag{7}$$

Transforming them into real-space representation by Eqs. (2) and (3), we obtain the input-output relations:

$$\tilde{a}_r(t) = \tilde{a}_{r-t}(0) - i\sqrt{\Gamma}\theta(r)\theta(t-r) d(t-r)\ , \tag{8}$$

$$\tilde{b}_r(t) = \tilde{b}_{r-t}(0) - i\sqrt{2\gamma_p}\theta(r)\theta(t-r) n_d(t-r)\ , \tag{9}$$

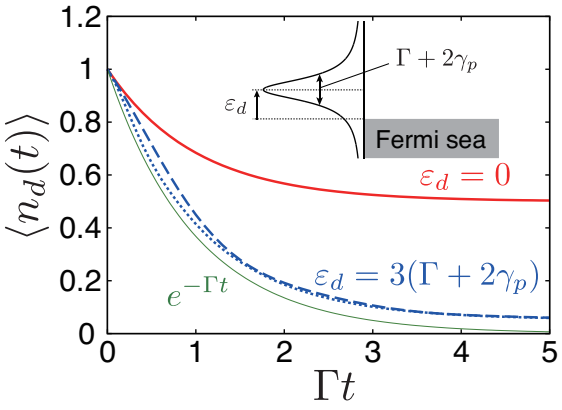

FIG. 2: Time evolution of the quantum dot population $\langle n_d(t)\rangle$, varying the dot energy ε_d: $\varepsilon_d = 0$ (red solid line), $\varepsilon_d = 3\Gamma$ without dephasing (blue dashed line) and $\varepsilon_d = 3(\Gamma + 2\gamma_p)$ with dephasing (blue dotted line), where $\gamma_p = \Gamma$ is assumed. We note that for $\varepsilon_d = 0$ the population is independent of γ_p. The exponential decay, $e^{-\Gamma t}$, is also plotted for reference (thin green solid line). Inset: The energy diagram of the quantum dot and the Fermi sea. The dot energy is centered at ε_d and has a linewidth of $\Gamma + 2\gamma_p$.

where $\theta(t)$ is the Heaviside step function. For $0 < r < t$, these input-output relations combine the output field $\tilde{a}_r(t)$ ($\tilde{b}_r(t)$) with the input field $\tilde{a}_{r-t}(0)$ ($\tilde{b}_{r-t}(0)$) at the initial time.

Next, we calculate the population of the quantum dot $\langle n_d(t)\rangle = \langle\psi(0)|n_d(t)|\psi(0)\rangle$ as a function of time. The equation of motion for the dot operator is derived for $t > 0$:

$$i\dot{d}(t) = \varepsilon_d d(t) + \sqrt{\Gamma}\tilde{a}_0(t) + \sqrt{2\gamma_p}(d(t)\tilde{b}_0(t) + \tilde{b}_0^\dagger(t)d(t)) \ . \tag{10}$$

The formal solution of this equation is obtained as:

$$d(t) = e^{-i\tilde{\varepsilon}_d t}d(0) - i\sqrt{\Gamma}\int_0^t dt' e^{i\tilde{\varepsilon}_d(t'-t)}\tilde{a}_{-t'}(0) - i\sqrt{2\gamma_p}\int_0^t dt' e^{i\tilde{\varepsilon}_d(t'-t)}(d(t')\tilde{b}_{-t'}(0) + \tilde{b}_{-t'}^\dagger(0)d(t')) \ , \tag{11}$$

where $\tilde{\varepsilon}_d = \varepsilon_d - i\Gamma/2 - i\gamma_p$. By combining this with the input-output relations, the population of the quantum dot is calculated as:

$$\langle n_d(t)\rangle = e^{-\Gamma t} + \delta n_d(t) \ , \tag{12}$$

$$\delta n_d(t) = \frac{\Gamma}{2\pi}\int_{-\infty}^0 dk \frac{1}{(k-\varepsilon_d)^2 + (\Gamma/2+\gamma_p)^2} \times \left[\frac{\Gamma + 2\gamma_p}{\Gamma}(1 - e^{-\Gamma t}) + f(t) + f(t)^*\right] \ , \tag{13}$$

$$f(t) = \frac{k - \varepsilon_d + i\Gamma/2 + i\gamma_p}{k - \varepsilon_d + i\Gamma/2 - i\gamma_p}(e^{-\Gamma t} - e^{(-ik + i\varepsilon_d - \Gamma/2 - \gamma_p)}) \ . \tag{14}$$

Here, we have used the fact that $\langle\tilde{a}_{r-t}(0)\rangle = \langle\tilde{b}_{r-t}(0)\rangle = 0$, $\langle a_k^\dagger(0)a_{k'}(0)\rangle = \theta(-k)\delta(k-k')$ and $\langle b_{-t'}^\dagger(0)b_{-t''}(0)\rangle = 0$ $(t', t'' > 0)$.

In Fig. 2, we plot $\langle n_d(t)\rangle$ as a function of t for several values of the dot energy ε_d. The population decays exponentially and approaches $1/2 - \tan^{-1}(\varepsilon_d/(\Gamma/2+\gamma_p))/\pi$ in the limit of $t \to \infty$. Note that the dot population does not decay completely due to the finite overlap in energy between the dot level and the Fermi sea. (see the inset of Fig. 2). For complete injection of one electron, the condition $\varepsilon_d \gg \Gamma/2 + \gamma_p$ is required.

IV. DENSITY MATRIX

The injected single electron wave packet is characterized by the density matrix:

$$\rho(r, r', t) = \langle\tilde{a}_{r'}^\dagger(t)\tilde{a}_r(t)\rangle \ . \tag{15}$$

Using the input-output relation of Eq. (6), this density matrix can be separated into two parts: $\rho(r, r', t) = \rho_0(r, r', t) + \delta\rho(r, r', t)$, each of which is defined as:

$$\rho_0(r, r', t) = \langle\tilde{a}_{r'-t}^\dagger(0)\tilde{a}_{r-t}(0)\rangle \ , \tag{16}$$

$$\delta\rho(r, r', t) = \Gamma\theta(r)\theta(r')\theta(t-r)\theta(t-r')C(t-r, t-r') \ , \tag{17}$$

where $C(t, t') = \langle d^\dagger(t')d(t)\rangle$.

Our objective is to probe the indistinguishability of electron wave packets. Experimentally, this is detected by colliding two such electrons at the location of a QPC after their propagation along opposite edges of a quantum Hall bar (as in the experiment of Ref. 12) and by measuring the zero frequency current-current correlations. This constitutes the electronic counterpart of the HOM experiment of quantum optics. As the first part $\rho_0(r, r', t)$ corresponds to the density matrix without electron injection, which does not contribute to the excess noise measurement in the HOM experiment, we focus on the second part $\delta\rho(r, r', t)$ in the range of $0 < r < t$ and $0 < r' < t$. From Eq. (17), this is achieved by calculating the correlation function of the dot $\langle d^\dagger(t')d(t)\rangle$. For $t' < t$, the equation of motion for this correlation function is derived:

$$i\frac{d}{dt}C(t, t') = \tilde{\varepsilon}_d C(t, t') + \frac{\Gamma}{2\pi}\int_{-\infty}^0 dk e^{-ikt}\frac{e^{ikt'} - e^{i\tilde{\varepsilon}_d^* t'}}{k - \tilde{\varepsilon}_d^*} \ , \tag{18}$$

With the solution:

$$C(t, t') = e^{-i\tilde{\varepsilon}_d(t-t')}\langle n_d(t')\rangle + \delta C^>(t, t') \ , \tag{19}$$

$$\delta C^>(t, t') = \frac{\Gamma}{2\pi}\int_{-\infty}^0 dk \frac{e^{-ikt'}}{(k-\varepsilon_d)^2 + (\Gamma/2+\gamma_p)^2} \times (e^{-ik(t-t')} - e^{-i\tilde{\varepsilon}_d(t-t')})(e^{ikt'} - e^{i\tilde{\varepsilon}_d^* t'}) \ . \tag{20}$$

In a similar way, the correlation function is calculated for $t' > t$:

$$C(t,t') = e^{i\tilde{\varepsilon}_d^*(t'-t)}\langle n_d(t)\rangle + \delta C^<(t,t') \ , \tag{21}$$

$$\delta C^<(t,t') = (\delta C^>(t',t))^* \ . \tag{22}$$

By combining these results with Eqs. (12)-(14) and (17), one can calculate the density matrix $\delta\rho(r,r')$ for arbitrary sets of the parameters.

In the following discussion, we assume for simplicity that the energy level ε_d measured from the Fermi energy is much larger than its linewidth (Γ and γ_p) to realize the complete injection of a single electron. Then, $\delta n_d(t)$, $\delta C^<(t,t')$, and $\delta C^>(t,t')$, which describe the effect of the Fermi sea in the edge channel, are evaluated:

$$|\delta n_d(t)| < \frac{5\Gamma/2+\gamma_p}{\pi\varepsilon_d} \ , \tag{23}$$

$$|\delta C^{<,>}(t,t')| \le \frac{2\Gamma}{\pi\varepsilon_d} \ , \tag{24}$$

for $t, t' \ge 0$ (for derivation, see Appendix B), and can be neglected when $\varepsilon_d/\Gamma, \varepsilon_d/\gamma_p \gg 1$, as we assume here. The correlation function $C(t,t')$ is then calculated using $\langle n_d(t)\rangle = e^{-\Gamma t}$:

$$C(t,t') = \begin{cases} e^{-i\tilde{\varepsilon}_d(t-t')-\Gamma t'}, & (t>t') \ , \\ e^{i\tilde{\varepsilon}_d^*(t'-t)-\Gamma t}, & (t<t') \ . \end{cases} \tag{25}$$

Now we switch to a frame moving at the Fermi velocity, $R = r - t$ and $R' = r' - t$. Then, in the limit of $t \to \infty$, the density matrix becomes independent of time. It is given by:

$$\begin{aligned} &\delta\rho(r,r',t) = \delta\rho(R',R) \\ &= \begin{cases} \Gamma e^{(-i\varepsilon_d-\Gamma/2-\gamma_p)(R'-R)}e^{\Gamma R'}, & (R<R'<0) \ , \\ \Gamma e^{(i\varepsilon_d-\Gamma/2-\gamma_p)(R-R')}e^{\Gamma R}, & (R'<R<0) \ , \\ 0 \ , & (\text{otherwise}) \ . \end{cases} \end{aligned} \tag{26}$$

The density matrix includes the whole information on the injected electrons. For instance, the shape of electron wave packet is obtained by the diagonal part of the density matrix:

$$f(R) = \delta\rho(R,R) = \Gamma e^{\Gamma R}\theta(-R) \ . \tag{27}$$

The injected electron has an exponential wave packet shape as expected. Note that this shape is determined only by Γ and is insensitive to the dephasing rate γ_p.[51] This implies that the dephasing effects are unobservable by a simple current measurement as achieved in Ref. 6. Another quantity which characterizes the injected electrons is their energy spectrum defined by:

$$\begin{aligned} S(k,t) &\equiv \langle a_k^\dagger(t)a_k(t)\rangle \\ &= \int \frac{drdr'}{2\pi}\langle \tilde{a}_{r'}^\dagger(t)a_r(t)\rangle e^{-ik(r-r')} \ . \end{aligned} \tag{28}$$

In the limit of $t \to \infty$, the spectrum is calculated using R and R' as $S(k,\infty) = \int dR\, dR' \delta\rho(R,R')e^{-ik(R-R')}$. From the density matrix of Eq. (26), we obtain the Lorentzian lineshape:

$$S(k) = \frac{1}{\pi}\frac{\Gamma/2+\gamma_p}{(k-\varepsilon_d)^2+(\Gamma/2+\gamma_p)^2} \ . \tag{29}$$

Here, we note as expected that the dephasing effects on the quantum dot affect the energy broadening of injected single electrons, in contrast with the wave-packet shape.

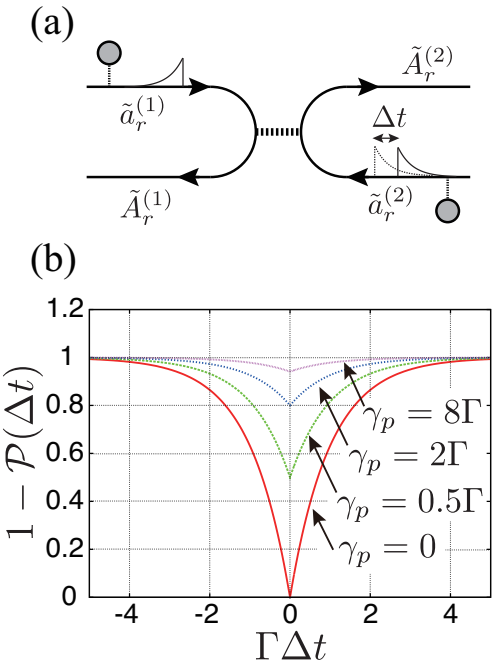

FIG. 3: (a) A collider setup for the fermionic Hong-Ou-Mandel experiment using two single-electrons generators, and (b) a plot of $1-\mathcal{P}(\Delta t)$, which is proportional to the excess current noise.

V. DETECTION OF DEPHASING WITH AN HONG OU MANDEL SETUP

We next consider the collider setup of the HOM experiment with two single-electron generators as shown in Fig. 3 (a). We assume that the quantum point contact at the center of Fig. 3 (a) has a transmission (reflection) probability of 1/2, playing the analog of a beam splitter in optics. We denote the two input edge channels with $a_r^{(1)}$ and $a_r^{(2)}$, respectively. Then, the two output edge channels are written as:[52]

$$A_r^{(1)} = (a_r^{(1)} + a_r^{(2)})/\sqrt{2} \ , \tag{30}$$

$$A_r^{(2)} = (a_r^{(1)} - a_r^{(2)})/\sqrt{2} \ . \tag{31}$$

In actual experiments, the measured quantity is the zero frequency excess noise:

$$S_{ii} = \int dt \int dt' \langle \Delta I_i(t)\Delta I_i(t')\rangle \ , \tag{32}$$

where $\Delta I_i(t) = I_i(t) - \langle I_i(t)\rangle$, I_i $(i = 1, 2)$ denotes the current in the output port i, and "excess" means that the contribution of the Fermi sea has been subtracted out. Because of the chiral nature of the propagation and the resultant propagation in the channel with a constant Fermi velocity, defining the total number of electrons observed in as $N_i = \int dr (A_r^{(i)})^\dagger A_r^{(i)}$, it turns out that the zero frequency excess current noise at the output port 1 is expressed as $S_{11} \propto \langle (\Delta N_1)^2\rangle$ $(\Delta N_1 = N_1 - \langle N_1\rangle)$. Using Eq. (30) and Eq. (31), we obtain:

$$\langle (\Delta N_1)^2\rangle = \frac{1 - \mathcal{P}(\Delta t)}{2} , \tag{33}$$

where Δt is the time delay between the two emitted electron wave packets and $\mathcal{P}(\Delta t)$ is defined by:

$$\mathcal{P}(\Delta t) = \int dr dr' \delta\rho(r, r', t)\delta\rho(r', r, t - \Delta t) . \tag{34}$$

From the density matrix of Eq. (26), we obtain:

$$\mathcal{P}(\Delta t) = \frac{\Gamma}{\Gamma + 2\gamma_p} e^{-\Gamma|\Delta t|} . \tag{35}$$

In Fig. 3 (b), we show a plot of $1 - \mathcal{P}(\Delta t)$, which is proportional to the excess current noise at the output port 1. If there is no dephasing ($\gamma_p = 0$), the excess noise is completely suppressed for a the simultaneous collision (time delay $\Delta t = 0$) between injected electrons. This is the manifestation of the antibunching due to the Fermi statistics of the injected electrons. As the pure dephasing rate γ_p increases, the degree of antibunching is reduced, and vanishes for $\gamma_p \gg \Gamma$. We note that $\mathcal{P} \equiv \mathcal{P}(\Delta t = 0)$ corresponds to the purity $\mathcal{P} = \mathrm{Tr}\rho^2$ of injected electrons, which has the simple form in our case:

$$\mathcal{P} = \frac{\Gamma}{\Gamma + 2\gamma_p} . \tag{36}$$

The purity approaches 1 for $\gamma_p \ll \Gamma$, leading to a perfect suppression of the excess noise ($S_{11} \propto 1 - \mathcal{P} = 0$), whereas the purity approaches 0 for $\gamma_p \gg \Gamma$, producing no sign of antibunching whatsoever.

We show another useful application of the present theoretical method. As dephasing occurs only in the quantum dot in our model, one can expect that an electron wave-packet injected at an earlier time suffers less dephasing. We can check this by considering wave-packets injected in the interval $0 \le t \le T_f$, where T_f is a filtering time. This time-filtering technique is widely used in quantum optics, and is also implementable in mesoscopic devices by dynamical control of the gate voltages or equivalently of the tunneling amplitude between the edge channel and the dot. Then, the excess current noise is related to the extended purity defined by:

$$\mathcal{P}_{T_f} = \frac{\mathrm{Tr}\rho^2}{(\mathrm{Tr}\rho)^2} = \frac{\int_{-T_f}^0 dR \int_{-T_f}^0 dR' \rho(R, R')\rho(R', R)}{(\int_{-T_f}^0 dR\, \rho(R, R))^2} . \tag{37}$$

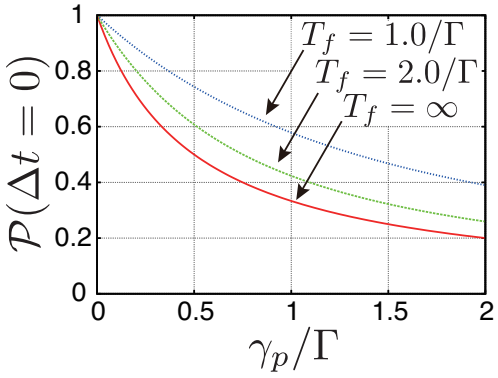

FIG. 4: The purity of generated single electrons after filtering in the period of $0 < t < T_f$.

Using our result for the density matrix, this quantity is calculated:

$$\mathcal{P}_{T_f} = \frac{2\Gamma^2}{(\Gamma + 2\gamma_p)(1 - e^{-\Gamma T_f})^2} \times \left[\frac{1 - e^{-2\Gamma T_f}}{2\Gamma} - \frac{e^{-\Gamma T_f - 2\gamma_p T_f} - e^{-2\Gamma T_f}}{\Gamma - 2\gamma_p}\right] . \tag{38}$$

In Fig. 4, we show $\mathcal{P}_{T_f}$ as a function of γ_p for $T_f = 1/\Gamma, 2/\Gamma, \infty$. Without time filtering ($T_f = \infty$), the purity decreases monotonically with γ_p. The purity is improved by the time filtering. The drawback of the time filtering is the possibility that no electron injection occurs from either or both of the two single-electron generators. The probability for successfully achieving an electron collision experiment is proportional to $(\mathrm{Tr}\rho)^2$, which amounts to 0.75 (0.4) for $T_f = 2/\Gamma$ $(1/\Gamma)$. For shorter filtering times, this probability decreases even more. This type of filtering scenario can be used to study the decoherence source in a tunable manner in the HOM experiment.

Finally, we briefly comment on other operations. In the opposite time-filtering scheme, i.e., in considering the wave-packet injected only at $t > T_f$, it is straightforward to show that the purity never changes from the one of the no-filtering case. It can also be shown that if the occupied dot state is raised at $t = 0$ with $\Gamma = 0$, is kept a while up to $t = T_f$, and is relaxed for $t > T_f$ by turning electron hopping finite ($\Gamma > 0$), the purity becomes the same as the one of the no-filtering case, because such an operation is expressed just by a shift of the origin of time.

VI. ASYMMETRIC WAVE PACKET COLLISIONS

Finally, we extend the present calculations to the case of an asymmetric wave-packet collision. In this context, asymetric can have two different meanings: on the one hand, the injection coupling between the dots and their respective edge channel may differ because of limitations

in nanolithography; on the other hand, since it is possible to adjust the dot energy levels with independent gates, controlled detuning is readily accessible. Both effects lead to asymetries of the shape of the electrons wave packets which can be analyzed with a Hong Ou Mandel interferometer.

We denote the decay rate, the pure dephasing rate, and the dot energy by Γ, γ_p, ε_d (Γ', γ'_p, ε'_d) for the single electron generator at the input channel 1 (2). One then obtains the excess noise, which is proportional to $1 - \mathcal{P}'(\Delta t)$, where

$$\mathcal{P}'(\Delta t) \equiv \int dR \int dR' \rho(R,R')\rho'(R'+\Delta t, R+\Delta t) \ , \tag{39}$$

and $\rho(R,R')$ and $\rho'(R,R')$ are the density matrix of the injected single electrons at the input channel 1 and 2, respectively. Using previous expressions, it is easy to obtain:

$$\mathcal{P}'(\Delta t) = \begin{cases} e^{-\Gamma'\Delta t}\mathcal{P}' & (\Delta t > 0) \\ e^{-\Gamma|\Delta t|}\mathcal{P}' & (\Delta t < 0) \end{cases} \tag{40}$$

$$\mathcal{P}' = \frac{2\Gamma\Gamma'}{\Gamma+\Gamma'} \times \frac{\tilde{\Gamma}}{\tilde{\Gamma}^2 + (\varepsilon_d - \varepsilon'_d)^2} \ , \tag{41}$$

where $\tilde{\Gamma} = \Gamma/2 + \Gamma'/2 + \gamma_p + \gamma'_p$. We discuss the above result as follows. First, assuming both zero detuning and dephasing, but different decay rates for the two injection processes, we obtain the same result as in Ref. 23: the HOM dip is asymmetric and lifted for zero time delay. Second, we notice that energy detuning alone leads to the lifting of the HOM dip. In both cases this reflects the fact that the two wave packets are distinguishable. Furthermore, we see that for arbitrary parameters of the two dots, information about the decay rate of the two dots can first be obtained by fitting the two (asymmetric) exponential sides of the dip. Knowing these decay rates, and by tuning the (constant) gate voltage on the dot so as to achieve $\varepsilon_d = \varepsilon'_d$, one could envision in practice to extract the quantity $\gamma_p + \gamma'_p$ which characterizes the dephasing to the whole setup. Alternatively, when carefully building a symmetric setup, the measurement of the dip for zero time delay is directly related to the energy detuning.

VII. CONCLUSION

In summary, we have discussed how the dephasing of an electron in a quantum dot due to an electromagnetic environment affects the coherence of injected electrons, using the input-output formulation which is inspired from quantum optics. We showed that the density matrix of the electrons which propagate on the chiral edge can be simply expressed in terms of the dot correlation function. This density matrix can be readily used to compute the fluctuations of the electron number – or the zero frequency noise – at either output of a beamsplitter collision experiment which constitutes the electrical analog of an HOM experiment, which is considered as a standard test of fundamental quantum mechanics. We have shown that the environmental noise does not change the spatial profile of the emitted electrons, whereas the spectrum and the degree of antibunching is definitely affected by the dephasing of the quantum dot. This treatment yields a rather simple explanation for the lifting of the HOM dip when the injected electrons suffer dephasing due to the their interaction with the electromagnetic environment located in the vicinity of the quantum dot. We have also shown that the time filtering helps to enhance the purity, and that a generalization of the present results to an asymetric setup is possible, with possible implication for measuring the energy detuning of the two injectors in actual experiments. Our approach provides not only a practical tool but also a clear and comprehensive picture of decoherence phenomena in single electron generation, and the results are directly connected to past and ongoing experiments on single electron generation which are performed in the quantum Hall effect.

Extensions to periodic gate voltage pulses, allowing for instance to perform hole-hole or electron-hole collisions could be envisioned, although some modifications of the present treatment would be required. More complex situations of interest, such as the fractionalization of charges[36,53] in quantum Hall bars containing several channels (which constitute yet another source of decoherence), or such as the consideration of similar dephasing effects when the quantum dot is connected to helical edge states in topological insulators[54,55] constitute important developments for future research. Note that such fractionalization scenario for decoherence as described in Ref. 36 does not apply in the present work, because we are dealing here with a filling factor one of the QHE which allows the presence of a single edge state only. In contrast, Ref. 36, which describes the experiment of Ref. 12 at filling factor two, points out that decoherence occurs because of Coulomb interactions with a (passive) second copropagating edge state. While other sources of decoherence cannot be ruled out in the present geometry, we believe that environmental noise on the injecting dot is likely to be a dominant source of dephasing.

Acknowledgments

We acknowledge helpful discussions with T. Jonckheere and J. Rech. T. K. was supported by JSPS KAKENHI Grant Number 24540316. T. M. acknowledges the support of ANR-2010-BLANC-0412 ("1 shot"). This work has been carried out in the framework of the Labex Archimède (ANR-11-LABX-0033) and of the A*MIDEX project (ANR-11-IDEX-0001-02), funded by the "Investissements d'Avenir" French Government program managed by the French National Research Agency (ANR).

Appendix A: Effect of the dot-environment coupling for $t < 0$

In this appendix, we show that the results of this paper are unaffected by the dot-environment coupling before single electron injection ($t < 0$). In our paper, the electron number in the dot is fixed as $n_d = 1$ for $t < 0$. By taking $n_d = 1$ and neglecting the electron hopping between the dot and a chiral edge channel, the environment for $t < 0$ is described by the Hamiltonian

$$H = \int dk k b_k^\dagger b_k + \sqrt{2\gamma_p}(\tilde{b}_0 + \tilde{b}_0^\dagger), \tag{A1}$$

$$\tilde{b}_r = \frac{1}{\sqrt{2\pi}} \int dk b_k e^{ikr}. \tag{A2}$$

By introducing a displaced field operator c_k defined by

$$c_k = b_k + \frac{1}{k}\sqrt{\frac{\gamma_p}{\pi}}, \tag{A3}$$

the Hamiltonian is diagonalized as

$$H = \int dk k c_k^\dagger c_k + \text{const.} \tag{A4}$$

Therefore, the vacuum state $|0\rangle$ for the field operator c_k is an eigenstate of H. The real-space representation of c_k is calculated as

$$\tilde{c}_r \equiv \frac{1}{\sqrt{2\pi}} \int dk c_k e^{ikr} = b_r + \frac{\sqrt{2\gamma_p}}{2\pi} \int dk \frac{e^{ikr}}{k}. \tag{A5}$$

In order to obtain physical results, we need to replace k with $k \pm i\eta$ in the denominator in the integral of Eq. (A5), depending on the boundary condition, where η is a positive infinitesimal quantity. We choose the boundary condition so that the input channel of the environment ($r < 0$) is the vacuum state of both of $\tilde{c}_r$ and $\tilde{b}_r$:

$$\tilde{c}_r|0\rangle = \tilde{b}_r|0\rangle = 0, \quad (r < 0) \tag{A6}$$

To satisfy this condition, we choose the replacement of $k \to k - i\eta$, and obtain

$$\tilde{c}_r = \tilde{b}_r + i\sqrt{2\gamma_p}\theta(r), \tag{A7}$$

where $\theta(r)$ is a step function. From this result, one can see that the dot-environment coupling affects only the output channel of the environment ($r > 0$). Because only the input channel is relevant in our paper (we used the fact that $b_r|0\rangle = 0$ for $r < 0$), the dot-environment coupling for $t < 0$ does not affect any results of our paper.

Appendix B: Derivation of Eqs. (23)-(24)

In this appendix, we prove the inequalities, Eq. (23) and Eq. (24). Using $|a+b| \le |a| + |b|$, $\Gamma \ge 0$, and $\gamma_p \ge 0$, one can evaluate the amplitude of $\delta n_d(t)$ from Eqs. (13)-(14):

$$\begin{aligned} |\delta n_d(t)| &\le \frac{\Gamma + 2\gamma_p}{2\pi} \int_{-\infty}^{0} dk \frac{1 - e^{-\Gamma t}}{(k-\varepsilon_d)^2 + (\Gamma/2+\gamma_p)^2} \\ &\quad + \frac{2\Gamma}{\pi} \int_{-\infty}^{0} dk \frac{|e^{-\Gamma t} - e^{-(\Gamma/2+\gamma_p)t}|}{(k-\varepsilon_d)^2 + (\Gamma/2-\gamma_p)^2} \\ &< \frac{1}{\pi}\left[\frac{\pi}{2} - \tan^{-1}\left(\frac{\varepsilon_d}{\Gamma/2+\gamma_p}\right)\right] \\ &\quad + \frac{2\Gamma}{\pi|\Gamma/2-\gamma_p|}\left[\frac{\pi}{2} - \tan^{-1}\left(\frac{\varepsilon_d}{|\Gamma/2-\gamma_p|}\right)\right]. \end{aligned} \tag{B1}$$

Using $\pi/2 - \tan^{-1}(x) \approx 1/x$ ($x \gg 1$), Eq. (23) is derived for $\varepsilon_d \gg \Gamma, \gamma_p$, By a similar way, one can evaluate the amplitude of $\delta C^<(t,t')$ and $\delta C^>(t,t')$:

$$\begin{aligned} |\delta C^{<,>}(t,t')| &\le \frac{\Gamma}{2\pi} \int_{-\infty}^{0} dk \frac{4}{(k-\varepsilon_d)^2 + (\Gamma/2+\gamma_p)^2}, \\ &= \frac{4\Gamma}{\pi(\Gamma+2\gamma_p)}\left[\frac{\pi}{2} - \tan^{-1}\left(\frac{\varepsilon_d}{\Gamma/2+\gamma_p}\right)\right], \end{aligned} \tag{B2}$$

leading to Eq. (24) for $\varepsilon_d \gg \Gamma, \gamma_p$.

* Electronic address: iyoda@noneq.c.u-tokyo.ac.jp

[1] R. H. Brown and R. Q. Twiss, Proc. of the Royal Society of London A **242**, 300 (1957); R. H. Brown and R. Q. Twiss, Proc. of the Royal Society of London A 243, 291 (1958).

[2] C. K. Hong, Z. Y. Ou, and L. Mandel, Phys. Rev. Lett. **59**, 2044 (1987).

[3] J. F. Clauser, Phys. Rev. D **9**, 853 (1974).

[4] F. J. Ahlers, O. F. O. Kieler, B. E. Sagŭol, K. Pierz, and U. Siegner, J. App. Phys. **100**, 093702 (2006).

[5] M. D. Blumenthal, B. Kaestner, L. Li, S. Giblin, T. J. B. M. Janssen, M. Pepper, D. Anderson, G. Jones, and D. A. Ritchie, Nat. Phys. **3**, 343 (2007).

[6] G. Fève, A. Mahé, J. Berroir, T. Kontos, B. Plaçais, D. C. Glattli, A. Cavanna, B. Etienne, Y. Jin, Science **316**, 1169 (2007).

[7] C. Leicht, P. Mirovsky, B. Kaestner, F. Hols, V. Kashcheyevs, E. Kurganova, U. Zeitler, T. Weimann, K. Pierz, and H. Schumacher, Semicond. Sci. Technol. **26**, 055010 (2011).

[8] S. Hermelin, S. Tanaka, M. Yamamoto, S. Tarucha, A.

Wieck, L. Saminadayar, C. Bäerle, and T. Meunier, Nature **477**, 435 (2011).
[9] R. P. G. McNeil, M. Kataoka, C. J. B. Ford, C. H. W. Barnes, D. Anderson, G. A. C. Jones, I. Farer, and D. A. Ritchie, Nature **477**, 439 (2011).
[10] S. Ol'khovskaya, J. Splettstoesser, M. Moskalets, and M. Büttiker, Phys. Rev. Lett. **101**, 166802 (2008).
[11] M. Moskalets and M. Büttiker, Phys. Rev. B **83**, 035316 (2011).
[12] E. Bocquillon, V. Freulon, J.-M. Berroir, P. Degiovanni, B. Plaçais, A. Cavanna, Y. Jin, and G. Fève, Science **339**, 1054 (2013).
[13] J. Dubois, T. Jullien, F. Portier, P. Roche, A. Cavanna, Y. Jin, W. Wegscheider, P. Roulleau, and D. C. Glattli, Nature **502**, 659 (2013).
[14] C. W. J. Beenakker, C. Emary, M. Kindermann, and J. L. van Velsen, Phys. Rev. Lett. **91**, 147901 (2003).
[15] J. Splettstoesser, M. Moskalets, and M. Büttiker, Phys. Rev. Lett. **103**, 076804 (2009).
[16] M. Moskalets, P. Samuelsson, and M. Büttiker, Phys. Rev. Lett. **100**, 086601 (2008).
[17] J. Splettstoesser, S. Ol'khovskaya, M. Moskalets, and M. Büttiker, Phys. Rev. B **78**, 205110 (2008).
[18] J. Keeling, A. V. Shytov, and L. S. Levitov, Phys. Rev. Lett. **101**, 196404 (2008).
[19] F. Battista and P. Samuelsson, Phys. Rev. B **83**, 125324 (2011).
[20] G. Haack, M. Moskalets, J. Splettstoesser, and M. Büttiker, Phys. Rev. B **84**, 081303(R) (2011).
[21] C. Grenier, R. Hervé, E. Bocquillon, F. D. Parmentier, B. Plaçais, J. M. Berroir, G. Fève, and P. Degiovanni, New J. Phys. **13**, 093007 (2011).
[22] T. Jonckheere, T. Stoll, J. Rech, and T. Martin, Phys. Rev. B **85**, 045321 (2012).
[23] T. Jonckheere, J. Rech, C. Wahl, and T. Martin, Phys. Rev. B **86**, 125425 (2012).
[24] M. Moskalets, G. Haack, and M. Büttiker, Phys. Rev. B **87**, 125429 (2013).
[25] M. Moskalets, Phys. Rev. B **88**, 035433 (2013).
[26] G. Haack, M. Moskalets, and M. Büttiker, Phys. Rev. B **87**, 201302(R) (2013).
[27] D. Ferraro, A. Feller, A. Ghibaudo, E. Thibierge, E. Bocquillon, G. Féve, Ch. Grenier, and P. Degiovanni, Phys. Rev. B **88**, 205303 (2013).
[28] Ch. Grenier, J. Dubois, T. Jullien, P. Roulleau, and D. C. Glattli, Phys. Rev. B **88**, 085302 (2013).
[29] J. Dubois, T. Jullien, C. Grenier, P. Degiovanni, P. Roulleau, and D. C. Glattli, Phys. Rev. B **88**, 085301 (2013).
[30] A. Mah'e, F. D. Parmentier, E. Bocquillon, J.-M. Berroir, D. C. Glattli, T. Kontos, B. Plaçais, G. Fève, A. Cavanna, and Y. Jin, Phys. Rev. B **82**, 201309(R) (2010).
[31] M. Albert, C. Flindt, M. Büttiker, Phys. Rev. B **82**, 041407(R) (2010).
[32] F. D. Parmentier, E. Bocquillon, J.-M. Berroir, D. C. Glattli, B. Plaçais, G. Fève, M. Albert, C. Flindt, and M. Büttiker, Phys. Rev. B **85**, 165438 (2012).
[33] E. Bocquillon, F. D. Parmentier, C. Grenier, J.-M. Berroir, P. Degiovanni, D. C. Glattli, B. Plaçais, A. Cavanna, Y. Jin, and G. Fève, Phys. Rev. Lett. **108**, 196803 (2012).
[34] P. Degiovanni, Ch. Grenier, and G. Fève, Phys. Rev. B **80**, 241307(R) (2009).
[35] G. Fève, P. Degiovanni, and Th. Jolicoeur, Phys. Rev. B **77**, 035308 (2008).
[36] C. Wahl, J. Rech, T. Jonckheere, and T. Martin, Phys. Rev. Lett. **112**, 046802 (2014).
[37] P. Roulleau, F. Portier, D. C. Glattli, P. Roche, A. Cavanna, G. Faini, U. Gennser, and D. Mailly, Phys. Rev. Lett. **100**, 126802 (2008).
[38] P. Roulleau, F. Portier, P. Roche, A. Cavanna, G. Faini, U. Gennser, and D. Mailly, Phys. Rev. Lett. **101**, 186803 (2008).
[39] C. Altimiras, H. le Sueur, U. Gennser, A. Cavanna, D. Mailly, and F. Pierre, Nature Physics **6**, 34 (2010).
[40] C. Altimiras, H. le Sueur, U. Gennser, A. Cavanna, D. Mailly, and F. Pierre, Phys. Rev. Lett. **105**, 226804 (2010).
[41] P.-A. Huynh, F. Portier, H. le Sueur, G. Faini, U. Gennser, D. Mailly, F. Pierre, W. Wegscheider, and P. Roche, Phys. Rev. Lett. **108**, 256802 (2012).
[42] B. Yurke and J. S. Denker, Phys. Rev. A **29**, 1419 (1984).
[43] M. J. Collett and C. W. Gardiner, Phys. Rev. A **30**, 1386 (1984).
[44] C. W. Gardiner, IBM J. Res. Dev. **32**, 127 (1988).
[45] D. Walls and G. J. Milburn, *Quantum Optics* (Springer, New York,, 1995).
[46] C. W. Gardiner and P. Zoller, *Quantum Noise* (Springer, New York, 2004).
[47] E. Iyoda, T. Kato, T. Aoki, K. Edamatsu, and K. Koshino, J. Phys. Soc. Jpn. **82**, 014301 (2013).
[48] J. Gabelli, G. Fève, J.-M. Berroir, B. Plaçais, A. Cavanna, B. Etienne, Y. Jin, D. C. Glattli Science **313**, 499 (2006).
[49] The quantum dot is assumed large enough that the spacing of its levels is dominated by confinement rather than Coulomb charging energy.
[50] One can extend the present formulation to the finite-temperature case in a straightforward way.
[51] If the coupling between the quantum dot and the edge state has an energy dependence, the dephasing may affect the shape of the wave packet.
[52] In general, there appears a phase factor in Eqs. (30)-(31). It, however, does not affect the present results, since it is only relevant when the system has interference paths.
[53] E. Bocquillon, V. Freulon, J.-M. Berroir, P. Degiovanni, B. Plaçais, A. Cavanna, Y. Jin, and G. Fève, Nature Communications **4**, 1839 (2013).
[54] A. Inhofer and D. Bercioux, preprint arXiv:1307.1198 (2013).
[55] P. P. Hofer and M. Büttiker, preprint arXiv:1307.1225 (2013).